Thermochromic SmNiO3-δ thin films deposited by magnetron sputtering and crystallized by soft-annealing in air

Zil Fernández-Gutiérrez, David Pilloud, Stéphanie Bruyère, Aurélien Didelot, Daria Kharkhan, Silvère Barrat, Fabien Capon

Version of Record: https://www.sciencedirect.com/science/article/pii/S1359646222002913
Manuscript_d215de086986c0cc67857a1d7813fe25

Thermochromic $SmNiO_{3-\delta}$ thin films deposited by magnetron sputtering and crystallized by soft-annealing in air

Zil Fernández-Gutiérrez[a*], David Pilloud[a], Stéphanie Bruyère[a], Aurélien Didelot[a], Daria N. Kharkhan[a], Silvère Barrat[a], Fabien Capon[a]

[a]Université de Lorraine, CNRS, IJL, F-54000 Nancy, France

*Email: zil.fernandez-gutierrez@univ-lorraine.fr

ABSTRACT

Samarium nickelate ($SmNiO_3$) exhibit a metal-insulator transition (MIT) around 120 °C and therefore appears to be an excellent candidate for a new generation of thermochromic solar absorbers. Nevertheless, this kind of perovskite is classically obtained under extreme conditions to stabilize the metastable Ni^{3+} oxidation state. Here, we show that $SmNiO_{3-\delta}$ thin films can be synthesized under soft-annealing as the habitual orthorhombic distorted perovskite structure. The layers were deposited by reactive magnetron co-sputtering and subsequently annealed for crystallization for 2 hours at 500 °C in air. Structural characterization was carried out using X-ray diffraction (XRD) and transmission electron microscopy (TEM) techniques, while optical and electrical properties were determined by Fourier transform infrared spectroscopy (FTIR) and the four-point probe method, respectively. The Ni^{3+} ion was confirmed by Electron energy loss spectroscopy (EELS). Finally, reversible thermochromic behavior was observed with an MIT temperature estimated at 138 °C and an IR contrast of 19%.

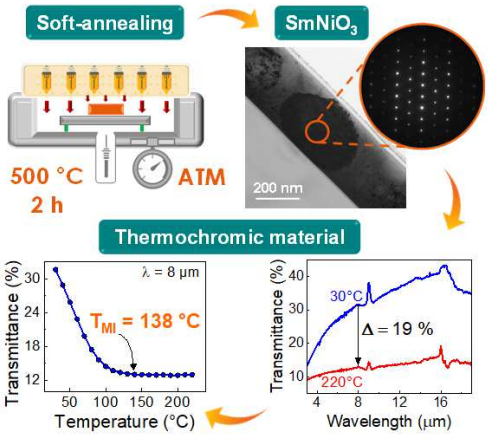

Keywords: *perovskites, nickelates, thermochromism, metal-insulator transition, thin films*

A large number of oxides crystallize in the perovskite structure RMO_3 (where *R* and M are two cations, a rare-earth and a transition metal, respectively). This structure allows a wide variety of lattice distortions and can accommodate plenty of chemical elements [1,2]. The present work is focused on the family of *rare-earth nickelates* with the chemical composition $RNiO_3$.

This material has been the subject of significant interest from the scientific community because of its exhaustive overview of functional properties. Nickelates exhibit rich physics, including charge ordering, strong electron-lattice coupling and long-period magnetically ordered states, all controlled by the interplay of crystal structure and electron correlations [3]. In addition, the existence of a metal-insulator transition temperature (T_{MI}) varying between -140 and 324 °C when the size of the rare-earth is reduced means these compounds are a highly versatile material [4]. Also, the phenomenon of thermochromism can be controlled by the presence of this metal-insulator transition (MIT). The latter is associated with optical changes such as light transmission, reflection, or emissivity in the infrared (IR) range. These give nickelates potential as materials which can be part of the new generation of smart absorber coatings for passive thermal regulation or infrared stealth applications [5,6].

However, developing them is challenging. Until recently, rare-earth nickelates required extreme annealing conditions (for crystallization) under high oxygen pressures (between 100-200 bar) to avoid oxygen loss and stabilize the Ni^{3+}, the least stable degree of nickel oxidation [4,7–11]. Another way to synthesize and stabilize this family of materials is through epitaxial growth which is favored by the parametric misfit between the substrate and the layer [12–16]. Even so, this kind of growth is strongly dependent on the quality of the process, the use of particular perovskite substrates with significant-high deposition temperatures and is also limited to ultra-thin layers [17].

The development of a simplified synthesis would be a meaningful step. Previous works have shown that it is feasible to obtain a thermochromic $NdNiO_{3-\delta}$ (T_{MI} = -68 °C) thin film without requiring high oxygen pressure annealing [18,19]. However, the tunability of the MIT for higher temperature values would need to be achieved to make applications possible that can be transposed to the industrial scale. The $SmNiO_3$ compound's T_{MI} is around 120 °C, making it an attractive material to study with a view to demonstrating why it could be used as a self-regulating selective layer in solar thermal collectors. Nevertheless, the radius

of Sm^{3+} is smaller than Nd^{3+} and its synthesis is more complicated due to a higher distortion that disfavors the metallic state and the Ni^{3+} stabilization [4,7,13]. Here, we report on the possibility of synthesizing thin crystallized *samarium nickelate* ($SmNiO_{3-\delta}$) films deposited on intrinsic silicon (100) substrates by reactive magnetron co-sputtering followed by soft-annealing in air.

The Sm-Ni-O thin films (290 nm thick) were elaborated from the 5-cm-diameter metallic targets of samarium and nickel (99.9% purity) co-sputtered in an argon-oxygen mixture (**Fig. 1(a)**). The Ar/O_2 ratio was set to 3 to assure a deposition in the reactive mode described by Capon *et al.* [18]. The base pressure within the vacuum chamber before the deposition was $1x10^{-5}$ Pa. The Ni and Sm targets were powered by a DC generator and a pulsed-DC power supply, respectively. The target/substrate distance was 10 cm. To achieve an Sm/Ni atomic ratio of 1 in the deposited films, the Sm sputtering current was held constant at 0.53 A, while the current dissipated on the Ni target was tuned and fixed at 0.13 A. The Sm/Ni atomic ratios were determined using an energy dispersive X-ray spectrometer (EDS) equipped in a scanning electron microscope (SEM) on a ZEISS GeminiSEM 500.

The working pressure was 0.5 Pa and the deposition time was 90 minutes. Finally, the substrates were mounted on a rotating substrate holder (6 rpm) to ensure a uniform distribution of Sm and Ni fluxes on the samples. No intentional heating was used during the film growth and the deposition temperature was close to 70 °C, thus inducing the formation of amorphous deposits (**Fig. 1(b)**).

A second step involves soft-annealing to crystallize these amorphous samples (**Fig. 1(c)**). The as-deposited thin films were annealed in air in a rapid thermal annealing (RTA) furnace (AS-One 100). The chamber was heated up to 500 °C in 18 s. After reaching the set temperature, the film was annealed for 2 hours.

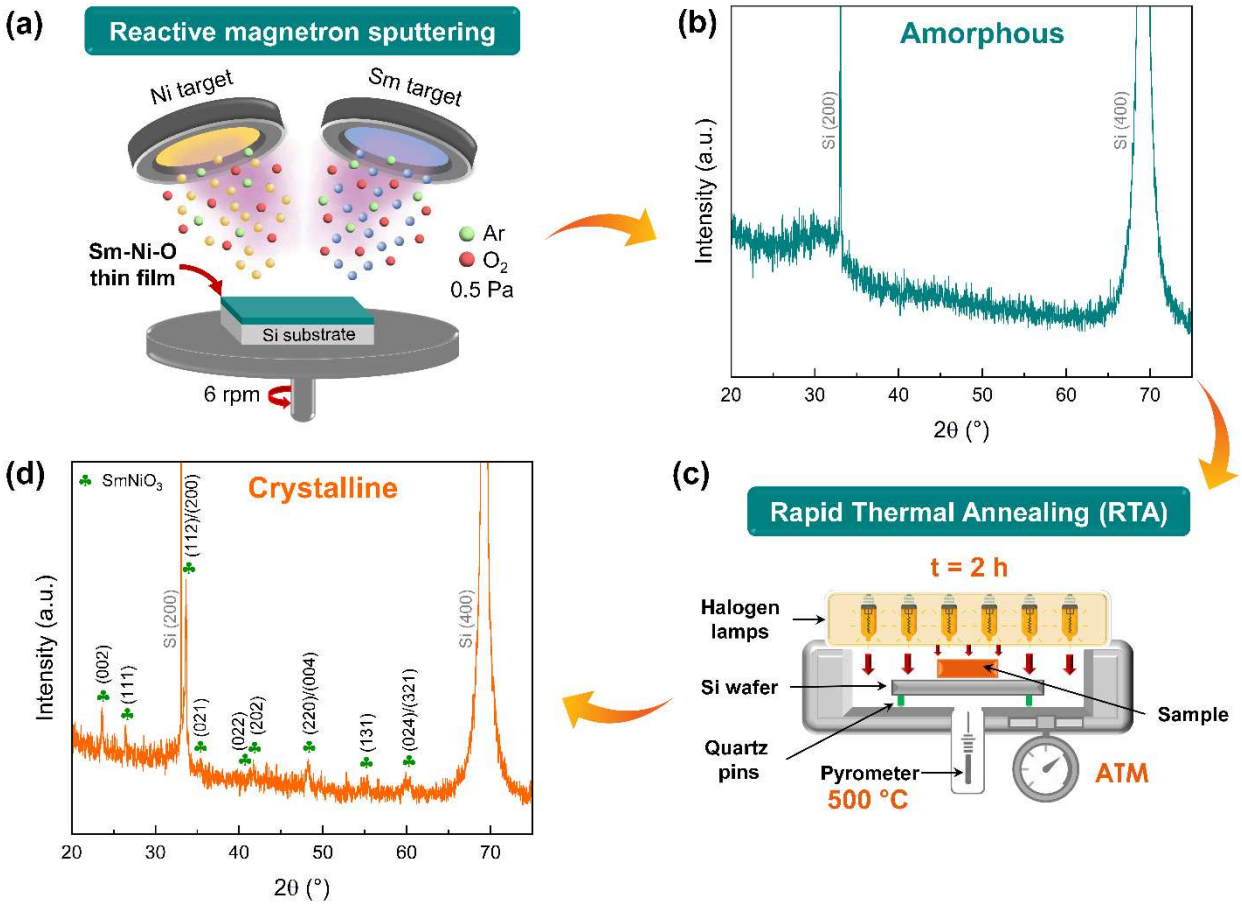

FIG. 1. Synthesis process and structural characterization of the Sm-Ni-O thin films. (a) Schematic of the co-sputtering system employed to deposit the layers. (b) X-ray diffractogram of the as-deposited film revealing its amorphous state. (c) Schematic of the RTA furnace used to crystallize the samples for 2 h at 500 °C in air. (d) X-ray diffractogram of the annealed and crystallized $SmNiO_{3-\delta}$ thin film. The (hkl) labels correspond to the $SmNiO_3$ diffraction pattern (PDF n° 51-0391).

X-ray diffraction (XRD, Cu $K\alpha_1$, λ = 0.15406 nm) was used to give the structural information. **Figures 1(b)** and **1(d)** show the XRD patterns recorded for as-deposited and air-annealed Sm-Ni-O thin films, respectively. As these figures show, the as-deposited sample was amorphous and, no other peaks except those of the silicon substrate were detected (**Fig. 1(b)**). On the other hand, the annealed sample at 500 °C for 2 hours exhibits many different peaks (**Fig. 1(d)**), which correspond to the orthorhombic phase of the $SmNiO_3$ perovskite structure (PDF n° 51-0391). Indeed, the most significant peak of $SmNiO_3$ could be identified at $2\theta = 33.6°$ but even the less intense ones are detected. The lattice parameters obtained were a = 0.528 nm, b = 0.539 nm and c = 0.752 nm, which are slightly smaller than those reported in previous works for $SmNiO_3$ (see **Table S1** in the supplementary material) [7,20]. It should be noted that there is no evidence of other oxide phases. However, compounds such as Sm_2O_3, SmO, NiO_2, NiO, Ni_2O_3 have already been observed in previous works dealing with $SmNiO_3$ deposited on silicon by magnetron sputtering [10,14].

These studies concluded that these oxides are stable phases under these growth conditions and also that they have been favored due to the absence of a close lattice match between the substrate and the film.

To find out more about the annealed sample, a transmission electron microscopy (TEM) study was performed with a JEOL ARM 200-Cold FEG. Cross-sectional TEM samples of films were prepared using a focused ion beam (FIB)-SEM dual beam system (FEI Helios Nanolab 600i). **Figure 2(a)** displays a TEM image of the film in which the presence of a grain with almost the same thickness as the layer (i.e. 270 nm) can be highlighted. The difference in contrast shown in **Fig. 2(a)** is the result of the different orientation of this grain concerning other crystallized areas. In this case, the grain is in a diffraction position and enables a bright-field image to be obtained (**Fig. 2(a)**) which shows everything that diffracts for a given orientation in a darker color. A selected area electron diffraction (SAED) was recorded to calculate and confirm the film's crystal structure. **Figure 2(b)** depicts the SAED pattern taken along the $[2\bar{2}1]$ zone-axis from the single-crystalline grain highlighted in **Fig. 2(a)**. Furthermore, we used Digital Micrograph^{TM} software to find, the spots of the planes (110), (012) and $(10\bar{2})$ with interplanar distances of 0.384, 0.312 and 0.309 nm, respectively. These results correspond with the XRD data and confirm the orthorhombic perovskite structure of $SmNiO_3$ with space group *Pbnm*.

Additionally, the compositional homogeneity within the film was verified by performing EDS mappings. From **Fig. 2(c)**, the uniform distribution of elements throughout the thickness of the film is corroborated. Only a blue layer which is richer in oxygen is of note and corresponds to a SiO_2 interlayer between the silicon substrate and the $SmNiO_{3-\delta}$ film. The atomic percentages measured were Sm = 18%, Ni = 19% and O_2 = 63%.

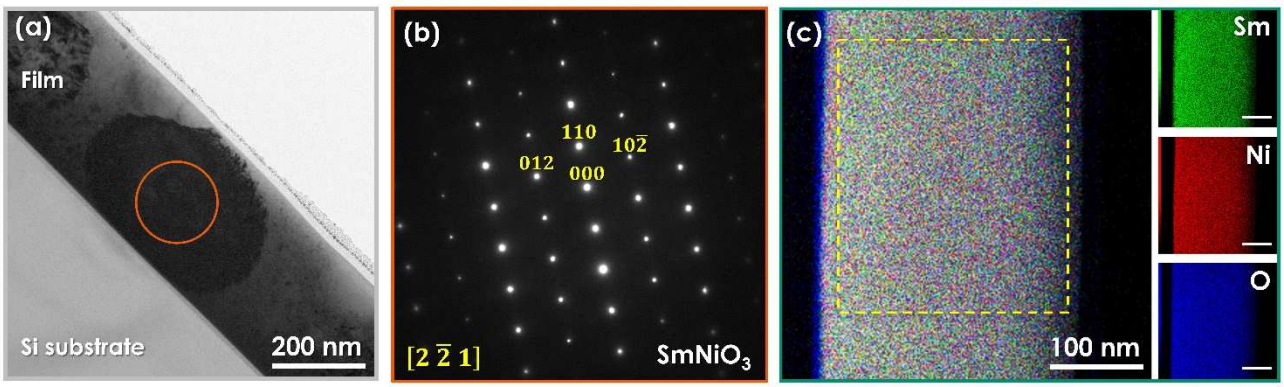

FIG. 2. Cross-section of the $SmNiO_{3-\delta}$ thin film annealed for 2 h at 500 °C in air. (a) Bright-field TEM image of the film showing an oriented grain in a diffraction position. (b) SAED pattern corresponding to the orange circle in (a). (c) EDS mapping of the diffracted area in (a). The atomic percentages measured in the area enclosed in the yellow dashed rectangle were Sm = 18%, Ni = 19% and O_2 = 63%.

It is important to note that, although only one area is shown in the present work, the TEM investigation confirmed the presence of many large grains (see **Fig. S4** in the supplementary material). These are encouraging results because, to the best of our knowledge, only neodymium nickelate ($NdNiO_{3-\delta}$) has been synthesized under non-drastic annealing in air (640°C for 3 days) [18]. Jaramillo *et al.* [10] emphasized the instability of nickelates and studied the particular case of $SmNiO_3$. They updated the thermodynamic phase stability diagram for $SmNiO_3$, which puts any annealing at atmospheric pressure into the unstable zone. Epitaxial growth is reported to be the only form that can be used below atmospheric pressure due to the low interfacial free energy which stabilizes this kind of growth and above all for substrates such as $LaAlO_3$ whose weakly compressive strain allows the $SmNiO_3$ phase formation [15]. Lastly, the intermediate conditions that they found for thin films involved a 24-hour annealing at 770 K (497 °C) and 100 bar O_2.

The oxygen stoichiometry is a vital aspect if we are to understand the crystallization of $SmNiO_{3-\delta}$ thin films by this annealing method. One of the benefits of high-pressure oxygen furnaces is that the sample is re-oxidized and crystallized. In particular, oxygen loss is avoided and the nickel is forced to remain at its least stable oxidation degree (Ni^{3+}). However, even with this method the mildest anneals reported take days and require a minimum temperature above 497 °C although soft-annealing is possible with the RTA furnace . Even in air, working in brief periods avoids an essential loss of oxygen in the sample which is synthesized as an oxide by magnetron sputtering (see **Fig. S7** in the supplementary material).

Nikulin *et al.* [21] have already investigated the influence of oxygen stoichiometry in the $NdNiO_{3-\delta}$ and $SmNiO_{3-\delta}$ systems. They noted that the oxygen index values (3-δ) systematically decrease with rising synthesis temperature and with reducing applied oxygen pressure, leading to the phase mixture of other binary oxides. To confirm the influence of oxygen deficiency in our samples, an Electron energy loss spectroscopy (EELS) analysis was carried out. **Figure 3(a)** depicts the O *K*-edge spectra in which can be highlighted the presence of the sharp peak at 529 eV corresponding to the nickel-oxygen hybridization (Ni *3d*−O *2p*) in its trivalent state. The latter is a signature in the electronic structure of nickelates [22–24].

Indeed, Abbate *et al.* [25] demonstrated how this peak disappears with increasing oxygen deficit in $LaNiO_{3-\delta}$. Also, in **Fig. 3(b)** is displayed the Ni *L*-edge spectra where the position of the peak Ni L_3 is in agreement with previous works that assigned the Ni^{3+} oxidation state around 855.6 eV [14,19,26,27]. Having already discussed these results, we can therefore state that the parameters used (2 hours at 500°C in air) allow the synthesis of $SmNiO_{3-\delta}$ thin films. Especially, having confirmed the phase by XRD and SAED pattern, the study of the electronic structure allows us to assume that the loss of oxygen is slight and the stabilization of Ni^{3+} is guaranteed.

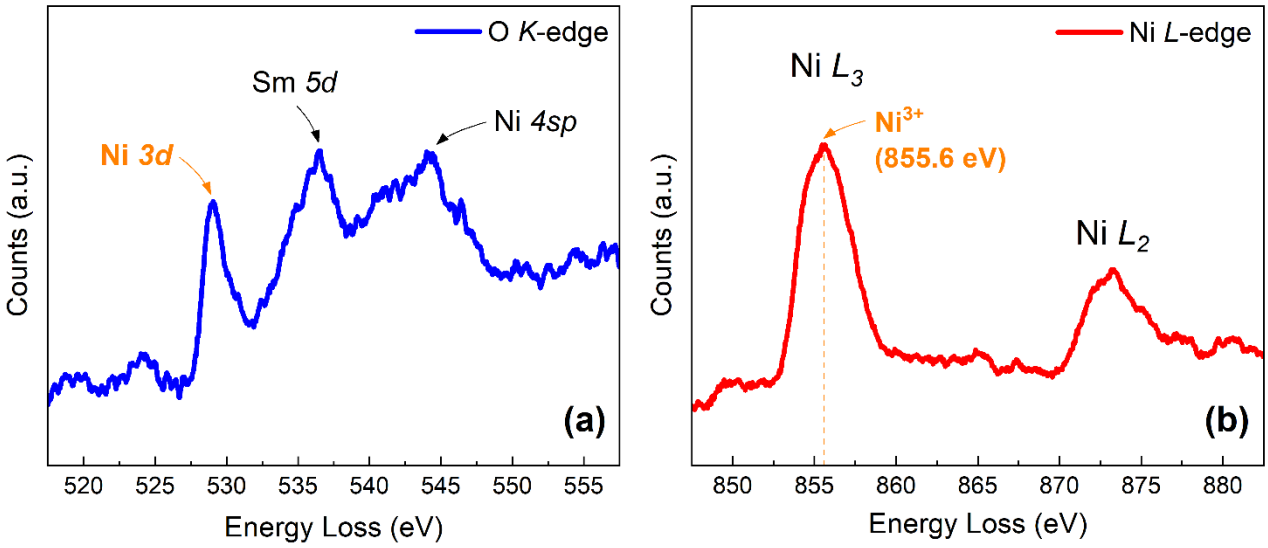

FIG. 3. Electron energy loss spectroscopy (EELS) analysis of the air-annealed sample at 500 °C for 2 h. (a) and (b) are the O *K*-edge and Ni *L*-edge EELS spectrum, respectively. The peaks associated with the orbital hybridization of Ni *3d*–O *2p* and the Ni^{3+} are indicated in orange color.

Electrical measurements can be used to confirm the metal-insulator transition and the thermochromic behavior. Nickelates are charge-transfer insulators in which an electron-electron interaction between the *d* band of the transition metal and the *p* band of the oxygen plays an important role [4,28,29]. Indeed, the straightening of the Ni-O-Ni bond angle (by increasing the temperature) increases the orbital overlap, thus stabilizing the metallic state over its semi-conducting counterpart (**Fig. 4(a)**) [4,30]. The study of the resistivity was carried out by a four-point probe method (see the supplementary material). **Figure 4(b)** presents the results obtained by heating and cooling the sample from 30 °C to 240 °C. Reversible behavior is observed whereby the slowing down of the resistance drops as the temperature increases. **Figure 4(c)** shows that no abrupt transition is visible although previous works on $SmNiO_3$ thin films on silicon substrates have made this aspect evident [14,16]. Also the small hysteresis is also observed in [10] and it could be associated

with a slight oxygen deficit. That is why we label our films "3-δ" (see **Fig. S7** in the supplementary material). Similar behavior to thermochromic VO_2 thin films is observed, whose MIT has been well studied and whose resistivity slightly decreases quasilinearly with temperature [31–34]. The metal-insulator transition temperature (T_{MI}) was determined using the line-line intersection method and could thus be estimated at 138 °C.

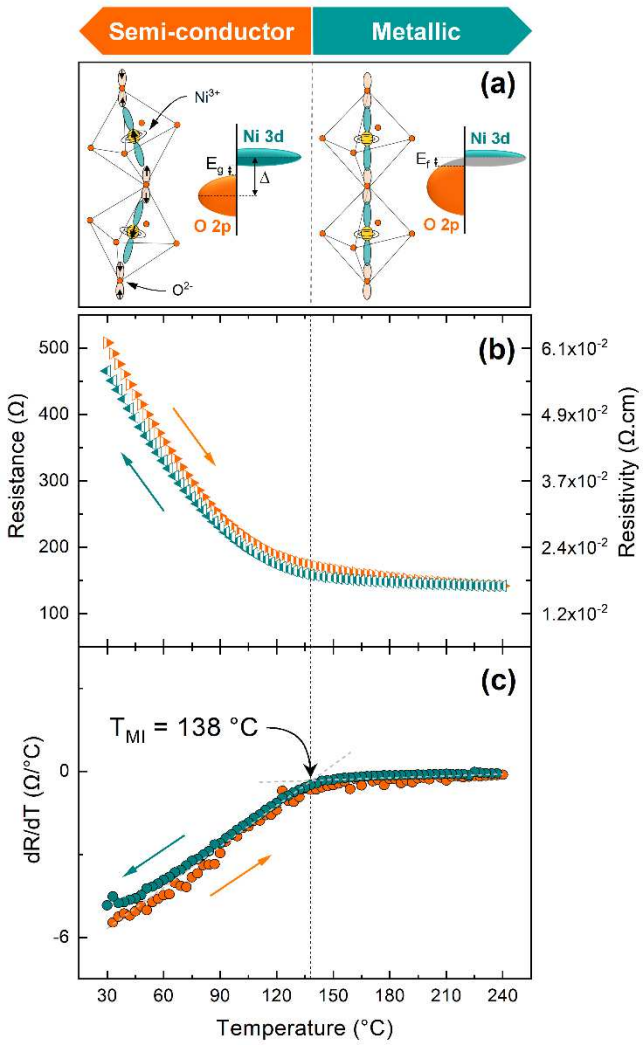

FIG. 4. Electrical behavior of the $SmNiO_{3-\delta}$ thin film annealed for 2 h at 500 °C in air. (a) Schematic of the straightening of the Ni-O-Ni bond angle (by increasing the temperature) which increases the orbital overlap, thereby easing charge transfer and stabilizing the metallic state. Figures based on previous works on $RNiO_3$ [4,30]. (b) Reversible evolution of the electrical resistance by heating and cooling the sample from 30 °C to 240 °C. (c) The line-line intersection method to determine the T_{MI}.

Regarding optical properties, infrared (IR) transmittance evolution of the annealed $SmNiO_{3-\delta}$ film was characterized at intervals corresponding to each rise of 10 °C in the heating ramp from 30 to 220 °C using a Linkam FTIR600. A Nicolet 6700 FTIR spectrometer was used to record the measurements between the

wavenumber range of 2.5-25 µm. The FTIR spectra *versus* temperature are depicted in **Fig. 5(a)**. The background is the IR light reaching the detector with the Linkam FTIR600 that contains a silicon substrate placed in the path of the IR beam. The absorption bands at 9.1 and 16.3 µm are assigned to the layer of SiO_2, which is included in the background taken at the beginning of the measurements. The band at 16.7 µm corresponds to the stretching of the Ni-O bond in NiO_6 octahedrons [35]. As can be seen, the screening effect helps show the considerable difference between the first and the last spectrum, both in their shape and their intensity. It is helpful regarding potential applications to report on the transmittance *versus* temperature in different transparency bands. Here, we chose the characteristic value of 8 µm since the screening effect *versus* temperature exhibits a significant contrast and, at this wavelength, the spectra are not altered by the absorption bands of silica or perovskites. Furthermore, this wavelength belongs to the band III (8–14 µm), where the atmospheric absorption is low. The transmittance progress of the latter is shown in **Fig. 5(b)**.

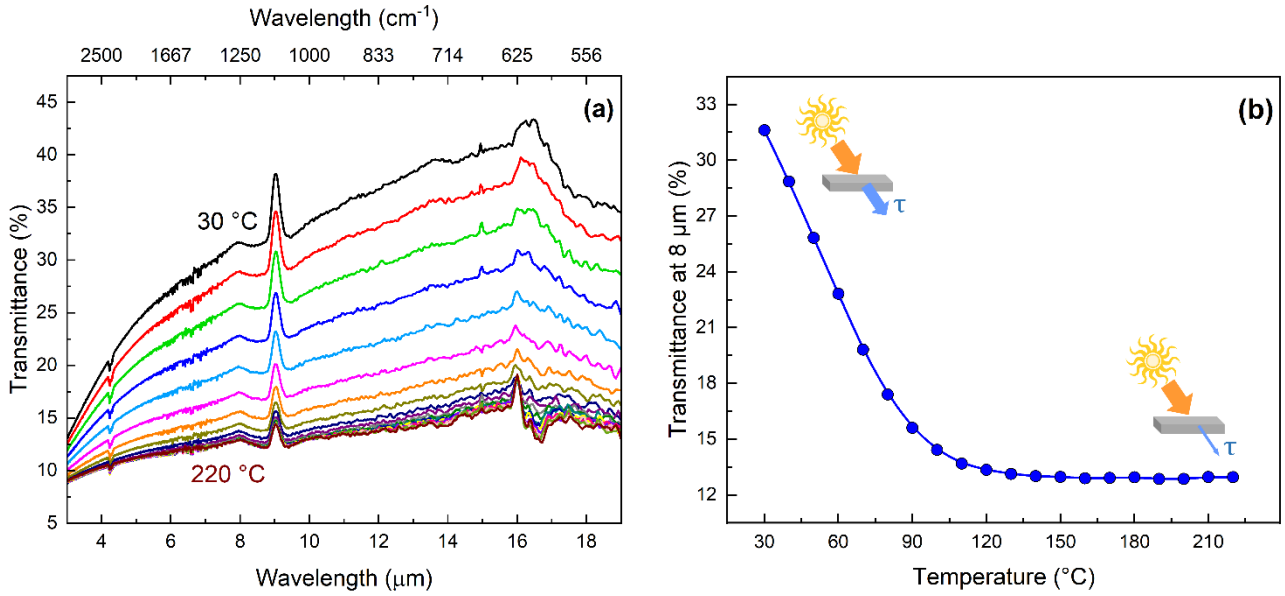

FIG. 5. Optical properties of the $SmNiO_{3-\delta}$ thin film annealed for 2 h at 500 °C in air. (a) Infrared (IR) transmittance evolution of the film in the heating ramp from 30 to 220 °C with a step of 10 °C. (b) IR transmittance performance at 8 µm *versus* temperature. The optical switching in thermochromic materials is illustrated in the schematics shown in the figure (τ: transmittance).

The decrease in transmittance ranges from approximately 32% at 30 °C to 13% at 220 °C. One phenomenon worthy of note is the stabilization of the transmittance between 130-140 °C and the fact that this does not decrease further despite the increasing temperature. The behavior described is characteristic of optical switching (in this case, about 19%) in thermochromic materials which move towards a less transparent state from low to high temperature. It should be noted that no change or modification is detectable in the visible

range. Nickelates have an optic gap located around 2.5 µm which makes it possible to observe a thermochromic behavior only in the infrared range (IR) [36].

It should also be stressed that a similar performance to that obtained by electrical measurements is noticeable. The relationship between a marked change in transmittance and electrical behavior under temperature has been observed in other nickelates [9,19,37]. In both cases, upon heating, the increase in density of charge carriers and the electronic interaction reveals the passage from an insulating to a metallic state and from a transparent material to a more opaque one [18]. This is a significant result because it represents a transmittance increase of more than 13 times that reported in the literature [38].

In summary, thermochromic $SmNiO_{3-\delta}$ thin films were synthesized by reactive magnetron sputtering followed by a soft-annealing in air. The deposition in the reactive mode and the use of an RTA system at 500 °C for 2 hours enabled crystalline $SmNiO_{3-\delta}$ thin films to be developed, showing a thermochromic effect of 19% at a wavelength of 8 µm with interesting electrical properties. The reversible metal-insulator transition (MIT) was estimated at close to 138 °C, which is slightly higher than the value reported for the bulk (120 °C) [39]. The presence of this metal-insulator transition is one of the most satisfactory results particularly if we consider the difficulties of synthesizing samarium nickelates thin films without extreme annealing conditions. Finally, having determined these properties meant we could consider the stabilization of the Ni^{3+} oxidation state and a non-significant loss of oxygen, making the synthesis of the orthorhombic phase of this nickelate possible. Subsequent work will consist of synthesizing solid solutions such as $Sm_{1-x}Nd_xNiO_3$ to tune the T_{MI} between -68 and 120 °C allowing to reach a T_{MI} at the ambient temperature. Producing this material in such a simple way paves the way for a new landscape of uses for nickelates, especially in industrial applications and as a self-regulating selective layer in solar thermal collectors.

SUPPLEMENTARY MATERIAL

See supplementary material for further details regarding synthesis optimization (compound mode during deposition and annealing conditions), additional structural characterization by TEM, comparison of the lattice parameters obtained in this work *vs.* with those published for $SmNiO_3$ bulk material, a description of the four-point probe method used, the reversibility and reproducibility of the metal-insulator transition,

oxygen evolution with annealing time and a comparison of air-annealed films of Sm-Ni-O in a conventional furnace *vs.* the RTA furnace.

ACKNOWLEDGEMENT

This work was supported partly by the French PIA project "Lorraine Université d'Excellence", reference ANR-15-IDEX-04-LUE. The authors acknowledge Emile Haye of Namur University for carrying out the oxygen measurements by XPS.

DATA AVAILABILITY

The data that support the findings of this study are available from the corresponding author upon reasonable request.

REFERENCES

[1] A.M. Glazer, Acta Crystallogr. Sect. B 28 (1972) 3384–3392.

[2] A.M. Glazer, Acta Crystallogr. Sect. A 31 (1975) 756–762.

[3] S. Middey, J. Chakhalian, P. Mahadevan, J.W. Freeland, A.J. Millis, D.D. Sarma, Annu. Rev. Mater. Res. 46 (2016) 305–334.

[4] J.B. Torrance, P. Lacorre, A.I. Nazzal, E.J. Ansaldo, C. Niedermayer, Phys. Rev. B 45 (1992) 8209–8212.

[5] D. Mercs, A. Didelot, F. Capon, J.F. Pierson, B. Hafner, A. Pazidis, S. Föste, R. Reineke-Koch, Energy Procedia 91 (2016) 84–93.

[6] C. Napierala, M. Edely, P. Laffez, L. Sauques, Opt. Mater. (Amst). 31 (2009) 1498–1501.

[7] P. Lacorre, J.B. Torrance, J. Pannetier, A.I. Nazzal, P.W. Wang, T.C. Huang, J. Solid State Chem. 91

(1991) 225–237.

[8] I. V. Nikulin, M.A. Novojilov, A.R. Kaul, A.F. Maiorova, S.N. Mudretsova, Mater. Res. Bull. 39 (2004) 803–810.

[9] F. Capon, P. Ruello, J.F. Bardeau, P. Simon, P. Laffez, B. Dkhil, L. Reversat, K. Galicka, A. Ratuszna, J. Phys. Condens. Matter 17 (2005) 1137–1150.

[10] R. Jaramillo, F. Schoofs, S.D. Ha, S. Ramanathan, J. Mater. Chem. C 1 (2013) 2455–2462.

[11] M. Kotiuga, Z. Zhang, J. Li, F. Rodolakis, H. Zhou, R. Sutarto, F. He, Q. Wang, Y. Sun, Y. Wang, N.A. Aghamiri, S.B. Hancock, L.P. Rokhinson, D.P. Landau, Y. Abate, J.W. Freeland, R. Comin, S. Ramanathan, K.M. Rabe, Proc. Natl. Acad. Sci. 116 (2019) 21992 LP – 21997.

[12] N. Ihzaz, S. Pignard, J. Kreisel, H. Vincent, J. Marcus, J. Dhahri, M. Oumezzine, Phys. Status Solidi 1 (2004) 1679–1682.

[13] F. Conchon, A. Boulle, R. Guinebretière, E. Dooryhée, J.L. Hodeau, C. Girardot, S. Pignard, J. Kreisel, F. Weiss, J. Phys. Condens. Matter 20 (2008) 145216.

[14] G.H. Aydogdu, S.D. Ha, B. Viswanath, S. Ramanathan, J. Appl. Phys. 109 (2011) 124110.

[15] S. Catalano, M. Gibert, V. Bisogni, O.E. Peil, F. He, R. Sutarto, M. Viret, P. Zubko, R. Scherwitzl, A. Georges, G.A. Sawatzky, T. Schmitt, J.M. Triscone, APL Mater. 2 (2014) 116110.

[16] B. Viswanath, G.H. Aydogdu, S.D. Ha, S. Ramanathan, Scr. Mater. 66 (2012) 463–466.

[17] S. Catalano, M. Gibert, J. Fowlie, J. Iñiguez, J.M. Triscone, J. Kreisel, Reports Prog. Phys. 81 (2018).

[18] F. Capon, D. Horwat, J.F. Pierson, M. Zaghrioui, P. Laffez, J. Phys. D. Appl. Phys. 42 (2009) 182006.

[19] A. Boileau, F. Capon, P. Laffez, S. Barrat, J.L. Endrino, R. Escobar Galindo, D. Horwat, J.F. Pierson, J. Phys. Chem. C 118 (2014) 5908–5917.

[20] P.F. Henry, M.T. Weller, C.C. Wilson, Chem. Mater. 14 (2002) 4104–4110.

[21] I. V. Nikulin, M.A. Novojilov, A.R. Kaul, S.N. Mudretsova, S. V. Kondrashov, Mater. Res. Bull. 39

(2004) 775–791.

[22] M. Medarde, A. Fontaine, J. García-Muñoz, J. Rodríguez-Carvajal, M. de Santis, M. Sacchi, G. Rossi, P. Lacorre, Phys. Rev. B 46 (1992) 14975–14984.

[23] B. Mundet, C. Domínguez, J. Fowlie, M. Gibert, J.M. Triscone, D.T.L. Alexander, Nano Lett. 21 (2021) 2436–2443.

[24] J.W. Freeland, M. Van Veenendaal, J. Chakhalian, J. Electron Spectros. Relat. Phenomena 208 (2016) 56–62.

[25] M. Abbate, G. Zampieri, F. Prado, A. Caneiro, J.M. Gonzalez-Calbet, M. Vallet-Regi, Phys. Rev. B - Condens. Matter Mater. Phys. 65 (2002) 1–6.

[26] Z. Fu, J. Hu, W. Hu, S. Yang, Y. Luo, Appl. Surf. Sci. 441 (2018) 1048–1056.

[27] K. Bilewska, E. Wolna, M. Edely, P. Ruello, J. Szade, Phys. Rev. B - Condens. Matter Mater. Phys. 82 (2010) 1–5.

[28] J. Zaanen, G.A. Sawatzky, J.W. Allen, Phys. Rev. Lett. 55 (1985) 418–421.

[29] T. Mizokawa, A. Fujimori, H. Namatame, K. Akeyama, N. Kosugi, Phys. Rev. B 49 (1994) 7193–7204.

[30] G. Catalan, Phase Transitions 81 (2008) 729–749.

[31] V. Melnik, I. Khatsevych, V. Kladko, A. Kuchuk, V. Nikirin, B. Romanyuk, Mater. Lett. 68 (2012) 215–217.

[32] J. Yoon, C. Park, S. Park, B.S. Mun, H. Ju, Appl. Surf. Sci. 353 (2015) 1082–1086.

[33] A.C. García-Wong, D. Pilloud, S. Bruyère, S. Mathieu, S. Migot, J.F. Pierson, F. Capon, Sol. Energy Mater. Sol. Cells 210 (2020) 1–7.

[34] T. Hajlaoui, N. Émond, C. Quirouette, B. Le Drogoff, J. Margot, M. Chaker, Scr. Mater. 177 (2020) 32–37.

[35] E.J. Baran, Catal. Today 8 (1990) 133–151.

[36] J.F. DeNatale, P.H. Kobrin, MRS Proc. 479 (1997) 145–152.

[37] F. Capon, P. Laffez, J.F. Bardeau, P. Simon, P. Lacorre, M. Zaghrioui, Appl. Phys. Lett. 81 (2002) 619–621.

[38] H. Miyazaki, S.I. Kikitsu, H. Suzuki, N. Adachi, T. Ota, J. Ceram. Soc. Japan 121 (2013) 10–12.

[39] L. Medarde, J. Phys. Condens. Matter 9 (1997) 1679–1707.